

# Accepted Manuscript

Interactions of 3D Mantle Flow and Continental Lithosphere near Passive Margins

R.J. Farrington, D.R. Stegman, L.N. Moresi, M. Sandiford, D.A. May

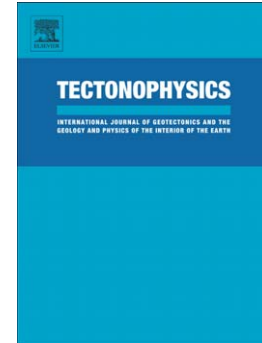
PII: S0040-1951(09)00567-8  
DOI: doi: [10.1016/j.tecto.2009.10.008](https://doi.org/10.1016/j.tecto.2009.10.008)  
Reference: TECTO 124764

To appear in: *Tectonophysics*

Received date: 18 February 2009  
Revised date: 2 September 2009  
Accepted date: 9 October 2009

Please cite this article as: Farrington, R.J., Stegman, D.R., Moresi, L.N., Sandiford, M., May, D.A., Interactions of 3D Mantle Flow and Continental Lithosphere near Passive Margins, *Tectonophysics* (2009), doi: [10.1016/j.tecto.2009.10.008](https://doi.org/10.1016/j.tecto.2009.10.008)

This is a PDF file of an unedited manuscript that has been accepted for publication. As a service to our customers we are providing this early version of the manuscript. The manuscript will undergo copyediting, typesetting, and review of the resulting proof before it is published in its final form. Please note that during the production process errors may be discovered which could affect the content, and all legal disclaimers that apply to the journal pertain.



# Interactions of 3D Mantle Flow and Continental Lithosphere near Passive Margins

R. J. Farrington<sup>a,\*</sup> D. R. Stegman<sup>b</sup> L. N. Moresi<sup>a</sup> M. Sandiford<sup>b</sup>  
D. A. May<sup>c</sup>

<sup>a</sup>*School of Mathematical Sciences, Monash University, Clayton, Victoria 3800, Australia*

<sup>b</sup>*School of Earth Sciences, The University of Melbourne, Carlton, Victoria 3010, Australia*

<sup>c</sup>*Institute of Geophysics, ETH Zurich, Zurich, Switzerland 8093*

---

## Abstract

We investigate the time evolution of 3D numerical models of convection in the upper mantle which incorporate both plate motions and thick continental lithosphere. The resultant flow in the upper mantle is driven by a combination of bottom heated convection and applied shear velocity boundary conditions that represents plate motion. Both the plate velocity and continental lithosphere topography are varied in a way to assess the general influence of 3D geometry as well as a more specific tectonic analogue of the Australian plate. Transient thermal events offshore of the trailing passive margin are observed and include plume migration, boundary layer instability growth at the passive margin and variations in surface heat flux. The geometry and plate velocity both play a significant role in controlling the magnitude and duration of these transient features. In particular, there are large differences between the different models in the oceanic region downstream of the trailing edge of the continent. At near-stationary plate speeds, cold linear downwelling sheets propagate away from the 3D edge of the continent, with regions offshore of the continents central axis localising hot cylindrical upwelling plumes. At very fast plate speeds, the shear flow is dominated by the plate motions. This causes regions neighbouring the trailing edge of the continent to produce broad, hot upwellings and the cold linear sheets to migrate around the continent. At moderate (2 cm/yr) plate speeds, oceanic lithosphere neighbouring the passive margin along the trailing edge of the continent is buffered by cold, downwelling instabilities sinking along the edges of the continental lithosphere. Such neighbouring regions are subjected to larger heat flux than for regions distant to the passive margin, yet also record smaller and less variable vertical surface velocities. These dynamics have implications for volcanism and surface topography, for which 3D aspects play a significant role.

*Key words:* Plate driven convection; small-scale convection; passive margins; lithospheric heat flux;

---

Proposed running head: 3D Models of Moving Continent Lithosphere

ACCEPTED MANUSCRIPT

---

\* [rebecca.farrington@sci.monash.edu.au](mailto:rebecca.farrington@sci.monash.edu.au)

## 1 **1 Introduction**

2 This study addresses the long-standing hypothesis that continental lithosphere and  
3 oceanic lithosphere operate fundamentally different from each other (Jordan, 1975;  
4 Pollack, 1986). In particular, regions of thickened continental lithosphere provide  
5 more resistance to heat escaping from the mantle underneath (Jordan, 1975; Pol-  
6 lack, 1986), and provide insulating constant heat flux boundary conditions to the  
7 mantle, rather than the constant temperature boundary conditions appropriate for  
8 oceanic lithosphere (Lenardic, 1995). This insulating effect can lead to heat accu-  
9 mulating beneath stationary continents as the underlying upper mantle gradually  
10 warms. Such a situation may be analogous to the separation of the Australian plate  
11 from former Gondwanaland. Australia was nearly stationary or very slowly moving  
12 for a long period of time prior to around 43 million years ago when fast northward  
13 drift commenced (Tikku and Cande, 1999). The continental insulation mechanism  
14 has also been proposed to generate very large pools of warmed material underneath  
15 supercontinents (Anderson, 1982, 1994). The interaction of large continents with  
16 an accumulation of heat within the underlying mantle has been previously investi-  
17 gated with 2D numerical models (Gurnis, 1988; Zhong and Gurnis, 1993; Lowman  
18 and Jarvis, 1995) as well as with analogue laboratory models (Guillou and Jaupart,  
19 1995). These early models treat continents as essentially 1D features (rafts on the  
20 surface driven by basal tractions from convective flow) that are compositionally  
21 buoyant and have higher viscosity which allows them to remain coherent over long  
22 (~Billion year) timescales. Similarly, rigid caps have been used to investigate the  
23 interaction between broad regions of warmed upper mantle and large continents in  
24 3D spherical geometry (Coltice et al., 2007).

25 The lithosphere underneath continental cratons is also thought to consist of a dis-  
26 tinct chemical composition that is both devolatilized (including dehydrated) as well  
27 as depleted of its mafic components (Jordan, 1975; Pollack, 1986). These material  
28 properties are thought to give it a strong and buoyant character, which helps it main-

tain long term stability. The thickness of the continental lithosphere varies, but is  
thickest underneath Archean cratons, in some places in excess of 300 km (i.e. much  
thicker than typical oceanic lithosphere). We designate the thickness, or depth, of  
this compositional boundary layer,  $\Delta Z_{CBL}$ . Later numerical models included for  
variable continental lithosphere thickness and studied the interactions between 2D  
continents embedded within the convecting mantle (O'Neill and Moresi, 2003;  
Cooper et al., 2004). The interactions between compositionally distinct thick con-  
tinental lithosphere and mantle convection in 3D geometry has received much less  
attention as recent studies in 3D treat plates as surface velocity boundary conditions  
(Nettelfield and Lowman, 2007).

One aspect of having variable  $\Delta Z_{CBL}$  is that large lateral temperature differences can  
occur between the continental lithosphere and adjacent upper mantle. In the case  
of a thick continental lithosphere moving at some speed through a passive man-  
tle, a secondary convective flow can be generated in the adjacent mantle along the  
trailing edge, otherwise referred to as Edge Driven Convection (EDC) (King and  
Anderson, 1998). EDC describes the time-dependent boundary layer instabilities  
resulting from lateral temperature variations across large ( $\geq 100$  km) discontinu-  
ous changes of lithospheric thickness. This flow can be considered as a result of  
2 different processes, the dynamic flow resulting from thermal buoyancy forces,  
and the shear flow resulting from plate motions. EDC should be sensitive to the  
sense of shear beneath moving continents. EDC has been used to explain intraplate  
volcanism in the absence of deep mantle plumes or extension and is thought to  
promote both volcanic activity (King, 2005) and anomalous dynamic topography  
(Shahnas and Pysklywec, 2004). Thus far, numerical models of EDC have been re-  
stricted to 2D and do not account for the inherent asymmetry between cold, linear  
downwelling sheets and hot, point-like cylindrical upwelling plumes as they would  
normally exist in 3D geometry. This motivates the first suite of numerical models  
for this study in which we investigate how thick continents interact with varying  
types of background mantle flows. In particular, we address whether EDC is signif-

Fig. 1.

58 ically different in 3D due to the inclusion of the natural asymmetries between the  
59 shape of upwellings and downwellings.

60 The Newer Volcanic Province (NVP) in South Eastern Australia has been proposed  
61 as an example of EDC volcanism, however many of the observables required for  
62 deep mantle plumes are absent in the NVP (King, 2007). Demidjuk et al. (2007)  
63 argued that EDC developed on the trailing edge of the continent, with an episodic-  
64 ity of approximately 10 Ma over the past 30 Ma. A recent analysis of shear wave  
65 splitting underneath Australia revealed a lithospheric structure that has variations  
66 in thickness orthogonal to the plate motion (Fishwick et al., 2008). Fishwick et al.  
67 (2008) propose a tiered lithospheric structure underneath Australia, as seen in Fig-  
68 ure 1, which shows progressively thinning towards the east, with lithosphere from  
69 central Australia having  $\Delta Z_{CBL} > 200$  km, followed by  $\Delta Z_{CBL} = 150 - 200$  km, and  
70 ending at the coastal section with  $\Delta Z_{CBL} \sim 100$  km.

71 It is not possible to model this type of lithospheric structure in 2D, as the discon-  
72 tinuous steps in  $\Delta Z_{CBL}$  do not occur in the same plane as the modeled flow. This  
73 aspect motivates the second suite of numerical models in this study which inves-  
74 tigate the effect of lateral variations of  $\Delta Z_{CBL}$  in directions only possible in 3D.  
75 The 3D geometry used in this study allows the flow from beneath the continent  
76 to freely advect past the trailing edge of the continent and interacting with the re-  
77 gional 3D convective planform beneath the oceanic lithosphere. This increase in  
78 complexity is of interest as 2D flow patterns can become unstable in this more re-  
79 alistic geometry. Planform stability and thermal asymmetries may be an important  
80 factor in the development and evolution of thermal instabilities along lithospheric  
81 discontinuities.

82 The work presented here, presumes by its initial condition, an insulated mantle un-  
83 derneath a continent. The influence of varying continental lithospheric topography,

84 as well as the velocity with which the continent moves are considered. In particu-  
85 lar, we quantify the thermal effects of the trailing passive margin of the continent  
86 on the neighbouring oceanic lithosphere. These thermal effects can be quantified  
87 through temperature differences in surface boundary layers and have direct conse-  
88 quences on surface observables (dynamic topography, heat flow, surface stresses) ,  
89 with deviations from adiabatic geotherms indicating an excess/deficit of heat. Im-  
90 portantly, these are the first models to employ a 3D geometry to explicitly address  
91 instabilities at the trailing edge of fast moving continents and the development of  
92 EDC, hypothesized to play a role in generating non-hotspot volcanism.

93 Using a 3D numerical model of mantle convection and building upon previous  
94 2D studies (King and Anderson, 1998; Shahnas and Pysklywec, 2004), this work  
95 is a generic study into the effects of a continent with an imposed plate speed on  
96 the underlying mantle, encompassing 3D aspects of both mantle convection and  
97 lithospheric discontinuities, and its resulting surface expression.

## 98 **2 Model Setup**

99 In this study, a series of 6 models employing 2 continental topographies with 3  
100 plate velocities was used. The goal of this paper is to determine the relative impor-  
101 tance which a 3D geometry has on the surface heat flux variations resulting from  
102 both the thermal convection and shearing components of flow present in the upper  
103 mantle. We model the interaction between continental lithospheric discontinuities,  
104 plate motions and thermal convection within a 3D bottom heated upper mantle.  
105 The continent is defined by a compositionally distinct material with a viscosity  $10^3$   
106 times larger than the reference mantle viscosity of  $10^{19}$  Pa s. The convecting upper  
107 mantle is parameterised by a Rayleigh number of  $10^6$ .

108 The model domain is defined by a Cartesian box of dimensions 5280 km x 5280 km  
109 x 660 km (8x8x1). The continent is defined using either a uniform or a tiered geom-

110 etry, as shown in Figure 2. The uniform geometry, with a continent of dimensions  
111 2640 km x 2640 km x 220 km, approximates the size of the Australian continent at  
112 220 km depth (Fishwick et al., 2008). The tiered geometry is defined by the union  
113 of 3 layers of thickness 100 km, 150 km and 220 km and width 3216 km, 2400 km  
114 and 1236 km respectively, resulting in the tiered form shown in Figure 2(ii). The  
115 symmetry of this model about the  $y$ -axis is leveraged by placing a free-slip bound-  
116 ary condition through  $y = 2400$  km. Couette boundary conditions were used to  
117 simulate plate motions by applying a velocity in the positive  $x$ -direction along the  
118 bottom boundary with periodic boundary conditions on the side walls and free-slip  
119 velocity boundary conditions on the back and front walls. Combination of free-  
120 slip and no-slip velocity boundary conditions on the top wall ensure no differential  
121 motion along the passive margin.

122 The initial condition for this model is a thermal statistically steady state mantle  
123 (similar to Cooper et al. (2004)) with periodic boundary conditions along the axis  
124 of plate motion and prescribed plate speed. The initial thermal steady state was de-  
125 termined using a model with the same geometry, material properties and boundary  
126 conditions as outlined above, with the exception of the imposed plate speed. This  
127 “no plate velocity” model was evolved in time until the surface heat flux variation  
128 was found to be within a tolerance of 1% for a significant period of time (25 Ma).

129 The interaction between plate velocity and flow resulting from thermal buoyancy is  
130 thought to result in EDC. The thermal buoyancy forces of interest here are a result  
131 of instabilities along the lateral temperature variations found across discontinuous  
132 changes in  $\Delta Z_{CBL}$ . Plate velocities within this study are assumed to originate from  
133 far field forces, and as such they are imposed as a surface velocity boundary condi-  
134 tion. The interaction of these forces with resulting flow velocities and the presence  
135 or absence of EDC is modelled by varying the imposed plate velocity with respect  
136 to the velocity resulting from thermal buoyancy forces, i.e. the vertical velocity.

137 The effect of an imposed plate speed on this initial steady state was studied by defin-

Table 1

Fig. 2.

138 ing regimes which were dominated, or balanced, by flow resulting from either the  
139 thermal buoyancy or the plate velocity. Three different plate speeds were studied  
140 with respect to these regimes (i) flow dominated by thermal buoyancy, (ii) flow bal-  
141 anced between thermal buoyancy and plate velocity (iii) plate velocity dominated.  
142 The characteristic plate speed for the three regimes was defined using the thermal  
143 steady state model (driven by only thermal buoyancy forces) as a reference model.  
144 From the reference model we computed the RMS value of the vertical component  
145 of velocity to obtain a reference speed of 2 cm/yr. From this, we selected the fol-  
146 lowing imposed plate speed for each of the three regimes (i) 0.2 cm/yr, representing  
147 thermal buoyancy dominated flow (ii) 2 cm/yr, allowing flow produced by thermal  
148 buoyancy and plate velocity of equivalent magnitude to interact and (iii) 20 cm/yr,  
149 producing plate velocity (shear) dominated flow.

150 The models were run for the length of time required to investigate the transient  
151 thermal state of the system. This time was defined as the time required for a parcel  
152 of mantle to travel from beneath the centre of the continent, past the trailing edge  
153 of the continent to the right wall boundary, through half of the domain in the  $x$ -  
154 direction. This transient time is dependent on the applied plate velocity and differs  
155 for the three imposed plate speeds as outline in Table 1. This model was solved  
156 using the Finite-Element Particle-In-Cell software package Underworld (Moresi  
157 et al., 2007) utilising only the finite element components of the package. The el-  
158 ement resolution used was 25 km in the horizontal direction and 18.75 km in the  
159 vertical direction. The velocity was scaled to the current surface RMS velocity for  
160 Earth found to be 3.7 cm/yr in the no-net-rotation reference frame taken from Table  
161 2a of Wu et al. (2008).

162 **3 Results**163 *3.1 Buoyancy Dominated Flow*

Fig. 3.

164 Figure 3 details results for a plate speed of 0.2 cm/yr taken at 3.4 Ma after the initi-  
165 ation of plate motion. Figure 3(a) shows hot material pooling beneath an insulating  
166 continent with small-scale instabilities at lithospheric discontinuities. Small-scale  
167 flow along the leading edge of the passive margin (left hand side) is shown to act  
168 as an anchor point for downwellings directing flow deeper into the mantle. Ther-  
169 mal plumes rising from the base of the upper mantle beneath the trailing edge of  
170 the passive margin (right hand side) perturbs the instability, directing flow upwards  
171 beneath the oceanic lithosphere.

172 Figure 3(b) shows the convection planform through the temperature field at a depth  
173 of 66 km, indicating that the inherent symmetry of the reference model is not  
174 broken with a plate speed of 0.2 cm/yr. The heat flux and velocity RMS also re-  
175 mains the same as that found in the reference model. This suggests that a low plate  
176 speed has a negligible effect on the initial condition and can therefore be consid-  
177 ered equivalent to the steady state reference model. Hot upwelling material is con-  
178 centrated offshore of the central continental regions, both along and perpendicular  
179 to the axis of plate motion. Cold downwelling sheets are focused offshore of the  
180 passive margin radiating from the continental edges. The cold downwellings con-  
181 tinuously migrate away from the continent towards the cold sheets which persist  
182 throughout the length of the simulation.

183 Figure 3(c) shows a conductive geotherm observed to 250 km depth within the  
184 continental thermal lithosphere for  $x = 2640$  km (blue) and  $x = 3300$  km (green),  
185 with the temperature differential across the thermal boundary layer ( $\Delta T_{BL}$ ) being  
186 0.7 of the temperature differential across the upper mantle ( $\Delta T$ ) and extending to a

187 depth of 320 km. The oceanic thermal lithosphere (aqua, magenta) persists to 100  
188 km depth with  $\Delta T_{BL} = 0.59\Delta T$ .

189 Figure 3(d) shows the cross section of the temperature field for the tiered conti-  
190 nental topography through  $y = 660$  km with lithospheric discontinuities again seen  
191 to anchor downwellings. Downwellings focused at the continental discontinuities  
192 propagate away perpendicular to the passive margin. Upwellings are focused off-  
193 shore of the central regions of the continent in both the  $x$ - and  $y$ -axis. The sub-  
194 continental geotherms of the tiered topography as shown in Figure 3(f) indicate  
195 that the depth of the thermal lithosphere is the same for both continental topogra-  
196 phies. The temperature drop across this conductive region is however smaller, with  
197  $\Delta T_{BL} = 0.68\Delta T$  for the continental and  $\Delta T_{BL} = 0.57\Delta T$  for the oceanic lithosphere.

### 198 3.2 *Buoyancy and Shear Flow Balanced*

Fig. 4.

199 Figure 4(a) taken 140 Ma after the initiation of a plate velocity of 2.0 cm/yr shows  
200 the hot insulated mantle located originally beneath the continent swept past the  
201 trailing edge of the passive margin resulting in a large scale thermal upwelling  
202 offshore. Lateral temperature differences along the passive margin result in time-  
203 dependent boundary layer instabilities forming an EDC cell. The passive margin  
204 at the leading edge of the continent shows a concentration of cold downwellings.  
205 The downwelling present at this passive margin blocks the movement of upwelling  
206 plumes directing flow deep into the upper mantle, cooling the upstream portion of  
207 the sub-continental mantle.

208 A plate speed of 2.0 cm/yr is sufficient to disrupt the symmetry of the convection  
209 planform as shown in Figure 4(b). Numerous cold downwellings are located off-  
210 shore of the leading edge of the continental margin with hot upwellings focused  
211 offshore of the trailing edge along the central axis. Two distinct upwellings can

212 be seen downstream at a distance of approximately 300 km and 800 km from the  
213 passive margin. The transportation of the insulated sub-continental mantle past the  
214 trailing edge of the passive margin results in a decrease in  $\Delta T_{BL}$  to  $0.6\Delta T$  as shown  
215 in Figure 4(c) for the continental thermal lithosphere compared to the previous  
216 small plate speed results. A variation in the depth and  $\Delta T_{BL}$  of the oceanic thermal  
217 lithosphere can also be seen with temperature gradients increasing to 100 km depth  
218 at (iv) but only 60 km at (vii).

219 The tiered continental topography, shown in Figure 4(d), results in time-dependent  
220 boundary layer instabilities along the passive margins. These instabilities also in-  
221 teract with the downwelling sheets radiating from lateral discontinuities within the  
222 passive margin, Figure 4(e). In the case of the trailing edge passive margin this  
223 results in a larger downwelling mass as seen in Figure 5 when compared to the  
224 uniform continental topography.

225 As shown in Figure 4(e), the interaction with shear flow resulting from the plate  
226 motions elongates downwelling sheets in comparison to those found for the slower  
227 plate speed. Hot upwellings are again focused along the central axis of the continent  
228 downstream of the passive margin. The sub-oceanic geotherms shown in Figure 4(f)  
229 again show a thermal lithosphere depth of  $\Delta T_{BL} = 0.6\Delta T$  in both locations (vi, vii).

Fig. 5.

230 Focusing on the area offshore of the trailing edge of the continent only, the evolution  
231 of the surface heat flux within different regions (outlined in Figure 2) are shown in  
232 Figure 5. Initial values for these regions indicate the partitioning of the total initial  
233 surface heat flux within the total downstream region. The regions adjacent to the  
234 passive margin (red and green) have the largest heat flux, being approximately 50%  
235 higher than the average steady state value. The regions distant to the passive margin  
236 maintain a smaller heat flux, being 50% smaller than the average steady state value  
237 for the total area.

238 Within the regions neighbouring the trailing edge of the continent (red and green)  
239 the heat flux shows some oscillations. Within the central region (green) for the first  
240 40 Ma, then between 90 Ma and 120 Ma a period between 12 Ma and 15 Ma is  
241 observed. Both regions at a distant to the passive margin show large oscillations  
242 throughout the evolution of the model.

Fig. 6.

243 The evolution of the near surface vertical velocity for both the uniform and tiered  
244 continental topographies across different regions within the area offshore of the  
245 trailing edge of the continent is shown in Figure 6. The vertical velocity for the adja-  
246 cent regions (red and green) remain relatively steady, showing a consistent increase  
247 with time. However these regions again show an oscillation that can be observed at  
248 a period between 12 Ma and 15 Ma. The distant regions (blue and magenta) show  
249 large fluctuations throughout the evolution. The region distant to the trailing edge  
250 passive margin for the uniform topography (solid, blue and magenta) fluctuate with  
251 a similar period (20 Ma), but differ in magnitude and phase throughout the first 60  
252 Ma. The trends of the tiered (dotted) continental topography between the distant  
253 outer regions and those central to the passive margin differ. The distant outer (blue)  
254 region maintains an oscillation with a period of approximately 15 Ma for the first  
255 80 Ma of plate motion. The amplitude of the oscillation then smoothly decays to a  
256 steady 0.4 cm/yr at 80 Ma and the periodicity breaks down, at 110 Ma an oscilla-  
257 tion of period  $\sim 15$  Ma returns. The tiered distant central region (magenta) follows  
258 a trend similar to its corresponding uniform model.

### 259 3.3 *Shear Flow Dominated Flow*

Fig. 7.

260 The temperature field with a plate speed of 20 cm/yr at a time 14 Ma after the ini-  
261 tiation of plate motion for the uniform and tiered continental topography is shown

262 in Figures 7(a) and (d) respectively. Shear velocity resulting from plate motion  
263 dominates the flow, inhibiting plumes rising from the base of the upper mantle and  
264 elongating the cold downwelling sheets. For the uniform topography this results  
265 in continuous large scale upwellings offshore of the trailing edge of the continent  
266 as shown in Figure 7(b). The elongated cool downwellings seen at lateral conti-  
267 nental discontinuities for the tiered topography (see Figure 7(e)) focus the thermal  
268 upwellings past the trailing edge of the continent along the central axis (with plate  
269 motion). In Figure 7(d), boundary layer instabilities along all passive margins are  
270 seen to be ‘pinched’ by the shear flow, directing upwellings in a downstream di-  
271 rection, with respect to the continent at both the leading and trailing edge of the  
272 continent. The increased cold downwellings present offshore of the trailing edge  
273 for the tiered topography result in a larger boundary layer instability along this  
274 passive margin, directing upwelling flow further offshore of the passive margin.

275 The shear flow has organised cold plumes originally radiating from the continental  
276 edges around the continent. As a consequence the sub-continental  $\Delta T_{BL}$  remains  
277 large as shown in Figures 7(c) and (e) in comparison to the moderate plate speed  
278 seen in Figure 4(b) where the continent overruns the cold downwellings originally  
279 located upstream to the continent. The sub-oceanic thermal lithosphere has the  
280 greatest  $\Delta T_{BL}$  of all plate speeds with both locations and topographies in excess  
281 of  $0.63\Delta T$ .

## 282 4 Discussion

283 The increased insulating effects of a deep continental lithosphere (Grigne et al.,  
284 2007) and its effect on the large scale flow (Guillou and Jaupart, 1995) can be seen  
285 in Figure 3 with heat pooling within the sub-continental mantle. When advected at  
286 sufficient plate speeds the insulated mantle can be swept downstream, increasing  
287 instabilities at  $\Delta Z_{CBL}$  discontinuities and focusing upwellings off-shore of the trail-  
288 ing edge of the continent as seen in Figure 4. Density driven thermal boundary layer

289 instabilities at  $\Delta Z_{CBL}$  direct flow for all plate speeds. At small plate speeds, the flow  
290 is directed downward into the upper mantle, with lateral flow only present when  
291 instabilities at the  $\Delta Z_{CBL}$  are perturbed by upwelling hot plumes. This flow can be  
292 considered as a reference model with flow advected by thermal buoyancy forces  
293 alone. At moderate plate speeds, with flow caused by both thermal buoyancy and  
294 plate motions, instabilities at the passive margin directing upwelling flow past the  
295 trailing edge of the continent are observed. The sub-continental mantle cools as the  
296 hot material is advected by plate motion as seen in Figure 4(a) and (d). Plate speeds  
297 exceeding those seen on Earth result in large thermal upwellings downstream of  
298 the passive margin, Figures 7(c) and (e). The original hot sub-continental mantle  
299 remains cool, as linear downwelling sheets are directed around the fast moving  
300 continent.

301 The inherent asymmetry between cold sheets and hot plumes within the 3D geom-  
302 etry modifies both the lateral length scale of the instabilities and the localisation  
303 of the resulting heat flow. The insulated mantle advected past the trailing edge of  
304 the continent and upwelled offshore is focused along the central axis of the conti-  
305 nent, at a distance from the continental discontinuities (Figure 4(a)). O'Neill and  
306 Moresi (2003) found downwellings with a 2D two-tiered continental topography  
307 are focused at lithospheric discontinuities. With the introduction of continental dis-  
308 continuities in the third dimension, the localisation of multiple downwelling sheets  
309 can be seen. While this is observed for both continental geometries, the effect is  
310 greater for the tiered geometry (with multiple  $\Delta Z_{CBL}$  discontinuities) as observed  
311 in the differing heat flux for continental topography adjacent to the passive mar-  
312 gin near the multiple  $\Delta Z_{CBL}$  discontinuities, Figure 5. The variation in heat flux  
313 with distance from  $\Delta Z_{CBL}$  discontinuities may be a key factor in the identification  
314 of EDC, with lateral variations in volcanic activity within regions offshore of the  
315 trailing edge of the continent. However more advanced models, taking into account  
316 a non-linear mantle and surface observables are required before these results can  
317 imply a stronger connection.

318 Heat flux and velocity trends for the regions neighbouring the trailing edge pas-  
319 sive margin show less variation when compared to the those at a distant. These  
320 steady regions indicate that the flow resulting from boundary layer instabilities at  
321  $\Delta Z_{CBL}$  discontinuities act as an anchor, buffering nearby regions from the large  
322 scale convection present within these regional models. The largest changes both in  
323 periodicity and long term smoothed trends occur in the distant regions, as a conse-  
324 quence of the continual migration of large scale features across these regions. The  
325 oceanic lithosphere next to the trailing edge passive margin measures the greatest  
326 heat flux as shown in Figure 5. However as seen in Figure 6, the vertical velocity  
327 within these regions is smaller than the more distant regions, thus buffering the re-  
328 gion from the cooling effect of the larger scale mantle flow. When viewed in the 3D  
329 regional setting, EDC can dominate the flow in the local (small/sub-upper mantle)  
330 length scale and may provide a mechanism for the mixing and melting of material  
331 originally beneath the continental craton. However a small frequency signal, which  
332 may indicate a local increase in heat flux or vertical velocity, could be smoothed out  
333 by the averaging used in this study. A potential example of this is the hot plumes  
334 discussed for both Figure 4(b) and 4(e) along the central axis of the continent along  
335 the direction of plate motion.

336 Continental lithosphere at velocity through the mantle can have an influence on  
337 continental geotherms (O'Neill and Moresi, 2003; Michaut and Jaupart, 2004),  
338 sub-continental geotherms (Cooper et al., 2004) and as shown here sub-oceanic  
339 geotherms. Results from plate velocities of 0.2 cm/yr, taken here to represent neg-  
340 ligible plate velocity, show geotherms as expected for oceanic regions with large  
341 temperature drops concentrated within the shallow lithosphere. This is also true for  
342 continental regions with geotherms registering a thick conducting lithosphere with  
343 a constant temperature differential across the depth of the continent and into the  
344 sub-continental thermal boundary layer. However with an increase in plate velocity  
345 to 2.0 cm/yr, an increase in the temperature drop across the sub-oceanic boundary  
346 layer is seen. This indicates the potential for super-adiabatic geotherms and there-

347 fore the occurrence of thermally driven events within this region. Conversely, the  
348 temperature drop across the sub-continental boundary decreases, indicating a cool-  
349 ing of the material below the continent. This study is restricted to the investigation  
350 of interactions between the upper mantle and  $\Delta Z_{CBL}$  discontinuities occurring dur-  
351 ing the transition from a stationary continent to a continent in motion. However, this  
352 cooling of the sub-continental mantle may have a significant effect on the instabil-  
353 ities forming along  $\Delta Z_{CBL}$  discontinuities as it approaches steady state, potentially  
354 decreasing the magnitude of these instabilities.

355 Depending on plate velocity the insulated sub-continental mantle can be advected  
356 past the trailing edge of the continent interacting with regional mantle convection.  
357 At sufficient plate speeds EDC can form, however the surface expression of this  
358 secondary mode of convection is undetermined within this study. Demidjuk et al.  
359 (2007) found the Newer Volcanic Province in Australia has a circulation timescale  
360 of order 10 Ma for material travelling from the base of the cratonic lithosphere un-  
361 derneath the Australian continent to the surface via volcanic activity. This timescale  
362 was also implicated by the presence of further volcanism within this region dating  
363 to between 19 and 30 Ma. In this study, with a plate speed of 2.0 cm/yr, we identify  
364 a periodicity of between 12 Ma and 15 Ma for both the heat flux and vertical ve-  
365 locity within the region adjacent to the trailing edge of the continent - the proposed  
366 location of EDC. The plate speed of 2 cm/yr used for this study is smaller than  
367 that of the Australian plate as it was chosen in order to illuminate the interaction  
368 between competing forces not in reference to a particular plate velocity. A The Aus-  
369 tralian plate is moving at over 6 cm/yr (O'Neill et al., 2005) and is therefore within  
370 the regime where buoyancy driven thermal velocities are of equivalent magnitude  
371 to those of the plate velocity. The factor of 3 difference between the model and the  
372 actual velocity of the Australian continent might reduce the periodicity found in the  
373 models, becoming closer to the observed 10 Ma timescale.

#### 374 4.1 *Future Directions*

375 The side wall velocity boundary conditions used in this model being periodic are  
376 sufficient for studying the initial, transient stage when a plate begins moving. In  
377 order to study the potential for longer lived steady state EDC, in the absence of  
378 an initially insulated sub-continental mantle, inflow/heat flux boundary conditions  
379 would be a requirement.

380 The isoviscous rheology used here allows for a first order approximation of the  
381 Earth's mantle. In order to study EDC in more detail and with reference to spe-  
382 cific surface expressions, a non-linear rheology, with temperature and strain rate  
383 dependence is required. The inclusion of a more complex and realistic rheology  
384 may affect the dynamics of the EDC outlined above. Using an isoviscous mantle  
385 is however an important step in understanding the interaction between the passive  
386 and active flow, particularly with the more complicated 3D convection planform  
387 and continental topographies included in this study.

## 388 5 **Conclusion**

389 Boundary layer instabilities are observed to act as anchors for small scale flow  
390 at passive margins when compositional and thermal discontinuities exist at depth  
391 within the upper mantle. The time dependent nature of these instabilities can be  
392 magnified and directed as a function of plate velocity. At sufficient speeds the ther-  
393 mally insulated sub-continental mantle can be swept downstream resulting in hot  
394 upwellings downstream of a passive margin. At Earth-like speeds, regional varia-  
395 tions indicate that flow anchored by continental discontinuities buffers the region  
396 adjacent to the trailing edge of the passive margin, resulting in smoother vertical  
397 velocities and heat flux within these areas, with an observed periodicity between 12  
398 Ma and 15 Ma. Fluctuations in surface heat flux are greater for the regions distant

399 to the passive margin, however the heat flux is largest within regions neighbour-  
400 ing the margin. In order to study this phenomena in detail a more realistic mantle  
401 rheology is required.

## 402 **Acknowledgments**

403 Software provided by AuScope Ltd, funded under the National Collaborative Re-  
404 search Infrastructure Strategy (NCRIS) an Australian Commonwealth Government  
405 Programme. Computational resources were provided by the National Computa-  
406 tional Infrastructure National Facility. This research was supported under Aus-  
407 tralian Research Council's Discovery Projects funding scheme (project number  
408 DP066325).

## 409 **References**

- 410 Anderson, D., Jun. 1982. Hotspots, polar wander, mesozoic convection and the  
411 geoid. *Nature* 297, 391–393.
- 412 Anderson, D., Jan 1994. Superplumes or supercontinents. *Geology* 22, 39–42.
- 413 Coltice, N., Phillips, B., Bertrand, H., Ricard, Y., Rey, P., 2007. Global warming  
414 of the mantle at the origin of flood basalts over supercontinents. *Geology* 35,  
415 391–394.
- 416 Cooper, C. M., Lenardic, A., Moresi, L., 2004. The thermal structure of stable  
417 continental lithosphere within a dynamic mantle. *Earth Planet Sci. Lett.* 222,  
418 807–817.
- 419 Demidjuk, Z., Turner, S., Sandiford, M., George, R., Foden, J., Etheridge, M., SEP  
420 30 2007. U-series isotope and geodynamic constraints on mantle melting pro-  
421 cesses beneath the Newer Volcanic Province in South Australia. *Earth Planet.*  
422 *Sci. Lett* 261 (3-4), 517–533.
- 423 Fishwick, S., Heintz, M., Kennett, B. L. N., Reading, A. M., Yoshizawa, K., 2008.

- 424 Steps in lithospheric thickness within eastern Australia, evidence from surface  
425 wave tomography. *Tectonics* 27 (4).
- 426 Grigne, C., Labrosse, S., Tackley, P. J., 2007. Convection under a lid of finite con-  
427 ductivity: Heat flux scaling and convection under a lid of finite conductivity: Heat  
428 flux scaling and application to continents. *Journal Geophysical Research* 112.
- 429 Guillou, L., Jaupart, C., 1995. On the effect of continents on mantle convection.  
430 *Journal of Geophysical Research B: Solid Earth* 100, 24217–38.
- 431 Gurnis, M., 1988. Large-scale mantle convection and the aggregation and dispersal  
432 of supercontinents. *Nature* 332, 695–699.
- 433 Jordan, T., 1975. The continental tectosphere. *Rev. Geophys. Space Phys* 13, pp.  
434 1–12.
- 435 King, S., 2005. Archean cratons and mantle dynamics. *Earth and Planetary Science*  
436 *Letters* 234, 1–14.
- 437 King, S., Anderson, D., AUG 1998. Edge-driven convection. *Earth Planet Sci. Lett.*  
438 160 (3-4), 289–296.
- 439 King, S. D., 2007. Hotspots and edge-driven convection. *Geology* 35 (3), 223–226.
- 440 Lenardic, A. Kaula, W., Dec 1995. Mantle dynamics and the heat-flow into the  
441 Earths continents. *Nature* 378, 709–711.
- 442 Lowman, J., Jarvis, G. T., 1995. Mantle convection models of continental collisions  
443 and breakup incorporating finite thickness plates. *Phys. Earth Planet. Int.* 88, 53–  
444 68.
- 445 Michaut, C., Jaupart, C., 2004. Nonequilibrium temperatures and cooling rates in  
446 thick continental lithosphere. *Geophysical Research Letters* 31.
- 447 Moresi, L., Quenette, S., Lemiale, V., Mériaux, C., Appelbe, B., Mühlhaus, H.-B.  
448 2007. Computational approaches to studying non-linear dynamics of the crust  
449 and mantle. *Physics of the Earth and Planetary Interiors* 163, 69–82.
- 450 Nettelfield, D., Lowman, J., 2007. The influence of plate-like surface motion on  
451 upwelling dynamics in numerical mantle convection models. *Physics of the Earth*  
452 *and Planetary Interiors* 161, 184–201.
- 453 O’Neill, C., Müller, R. D., Steinberger, B., 2005. On the uncertainties in hot spot

- 454 reconstructions and the significance of moving hot spot reference frames. *Geoc.*  
455 *Geophy. Geosys* 6.
- 456 O'Neill, C. J., Moresi, L., 2003. How long can diamonds remain stable in the con-  
457 tinental lithosphere? *Earth And Planetary Science Letters* 213, 43–52.
- 458 Pollack, H., Oct. 1986. Cratonization and thermal evolution of the mantle. *Earth*  
459 *and Planetary Science Letters* 80, 175–182.
- 460 Shahnas, M., Pysklywec, R., SEP 30 2004. Anomalous topography in the west-  
461 ern Atlantic caused by edge-driven convection. *Geophysical Research Letters*  
462 31 (18).
- 463 Tikku, A., Cande, S., 1999. The oldest magnetic anomalies in the Australian -  
464 Antarctic basin: are they isochrons? *J. Geophys. Res.* 104, 661–77.
- 465 Wu, B., Conrad, C., Heuret, A., Lithgow-Bertelloni, C., Lallemand, S., 2008. Rec-  
466 onciling strong slab pull and weak plate bending: The plate motion constraint on  
467 the strength of mantle slabs. *Earth and Planetary Science Letters* 272, 412–421.
- 468 Zhong, S., Gurnis, M., 1993. Dynamic feedback between an non-subducting raft  
469 and thermal convection. *Journal Geophysical Research* 98, 12219–32.

470 **FIGURE 1** A map of the Australian continent modified from Figure 9 of Fishwick  
471 et al. (2008). The location of the Newer Volcanic Province is shown in South-  
472 Eastern Australia. The thickness of the lithosphere is shown by colour. Dark green  
473 represents regions with a thickness greater than 200 km, light green represents re-  
474 gions between with a thickness between 150 and 200 km, yellow for regions  $\sim 100$   
475 km thick and cream for regions of  $\sim 50$  km thick. The 3D tiered structure at depth  
476 can be seen in the cross section. The coordinates used within this study and the  
477 plate motion vector are shown for reference.

478  
479 **FIGURE 2** A schematic of the model setup including coordinate system, domain  
480 and continental geometry, velocity and temperature boundary conditions and de-  
481 composition of the 3D surface area offshore of the trailing edge of the continent.  
482 The origin of the coordinate system is taken to be at the top front left corner of the  
483 domain, with  $z$  representing depth and equal to 0 at the surface. The continent is  
484 defined with either a (a) block or (b) tiered geometry. The oceanic lithosphere off-  
485 shore of the trailing edge of the continent has been decomposed into 4 individual  
486 region labelled 1 - 4, representing regions either adjacent (1,3) or distant (2,4) to  
487 the trailing edge passive margin and regions along the central axis (3,4) or distant  
488 (1,2) of the continent. The block geometry is defined as a rectangular prism of di-  
489 mensions 2640 km x 1320 km x 220 km. The tier geometry as shown in (b), with  
490 an exaggerated ( $\times 4$ ) vertical scale, is defined by the union of 3 rectangular prisms  
491 with a constant length of 2640 km, successively smaller depths of 220 km, 150 km  
492 and 100 km, and increasing widths of 1236 km, 2400 km and 3216 km respectively.  
493 The full domain is a 3D Cartesian box of length 5280 km, width 2640 km and depth  
494 660 km. The symmetry of the continental topography allows for a mirror/free slip  
495 front and back wall velocity boundary condition, cutting the computation required  
496 by half. Periodic boundary conditions are used along the left and right wall allow-  
497 ing for the imposed plate motions as for Couette flow. The imposed plate motion is  
498 enabled through a prescribed velocity in the positive  $x$ -direction along the bottom  
499 wall. A combination free-slip/no-slip velocity boundary condition is used along the

500 top wall, ensuring no differential motion between the continental and oceanic litho-  
501 sphere throughout the length of the passive margin. The no-slip region is marked in  
502 grey. The temperature is fixed at both the top and bottom wall with a temperature  
503 increase across the depth of the domain held constant at  $\Delta T$ .

504

505 **FIGURE 3** Simulation results for a plate speed of 0.2 cm/yr (models 1 and 2 in  
506 Table 1) taken at 3.4 Ma after the initiation of plate motion are representative of  
507 the pattern of instability growth seen throughout the length of the model. The di-  
508 rection and magnitude of plate motion is indicated by the arrow at the top centre  
509 of the figure. (a) Temperature field of the block continental topography for a cross  
510 section taken at  $y = 660$  km. Cold temperatures are represented with blue, hot  
511 with red. The line and arrow marked (i) indicate the location of the cross section  
512 shown in (b). (b) Planform of the temperature field for a cross section taken at 66  
513 km depth for the block continental topography. The line and arrow marked (ii) in-  
514 dicate the location of the cross section shown in (a). The rectangular area outlined  
515 (dashed line) represents the region used in calculating the geotherms shown in (c).  
516 The coloured arrows numbered (iii) to (vii) indicate the location of the geotherms  
517 shown in (c). These geotherms are taken as an average value with depth across only  
518 half the width of the domain, as outlined by the dashed lines at each coloured ar-  
519 row. As an example, the blue arrow marked (iii) corresponds to the blue geotherm  
520 in (c) and is calculated using the average temperature with depth at  $x = 2640$  km  
521 across the width from  $0 \text{ km} \leq y \leq 1320$  km. (c) Geotherms found beneath the con-  
522 tinent, along the trailing edge of the continent and beneath the oceanic lithosphere  
523 within the downstream region of the domain, defined by the dashed rectangle in  
524 (b). Geotherms were taken at  $x = 2640$  km (blue), 3300 km (green), 3960 km (red),  
525 4620 km (aqua) and 5280 km (magenta). (d)-(f) as for (a)-(c) with the tiered conti-  
526 nental topography.

527

528 **FIGURE 4** Simulation results for plate speeds of 2 cm/yr (models 3 and 4) at a  
529 time of 140 Ma from the initiation of plate motion as for Figure 3.

530

531 **FIGURE 5** Evolution of the normalised vertical heat flux with time (Ma) for both  
 532 a uniform (solid line) and tiered (dotted line) continental topography within the  
 533 downstream region at a depth of 50 km. The downstream domain is decomposed  
 534 into four regions using the location of the central trailing edge of the passive mar-  
 535 gin as a reference outlined in Figure 2. The vertical heat flux values are averaged  
 536 across the surface elements within a region and then normalised for the steady state  
 537 surface heat flux for the entire downstream domain. Red:  $1320 \text{ km} < x < 1980 \text{ km}$ ,  
 538  $0 \text{ km} < z < 66 \text{ km}$ , region (1). Green:  $1980 \text{ km} < x < 2640 \text{ km}$ ,  $0 < z < 660 \text{ km}$ ,  
 539 region (2). Blue:  $1320 \text{ km} < x < 1980 \text{ km}$ ,  $660 \text{ km} < z < 1320 \text{ km}$ , region (3).  
 540 Magenta:  $1980 \text{ km} < x < 2640 \text{ km}$ ,  $660 \text{ km} < z < 1320 \text{ km}$ , region (4).

541

542 **FIGURE 6** Evolution of the vertical velocity (cm/yr) with time (Ma) for both a  
 543 uniform (solid) and tiered (dotted) continental topography for the downstream re-  
 544 gion at a depth of 50 km. The downstream domain is decomposed into four regions  
 545 using the location of the central passive margin as a reference, outlined in Figure 2.  
 546 Vertical velocity are averaged across the individual regions. Red:  $1320 \text{ km} < x <$   
 547  $1980 \text{ km}$ ,  $0 \text{ km} < z < 66 \text{ km}$ , region (1). Green:  $1980 \text{ km} < x < 2640 \text{ km}$ ,  $0 \text{ km}$   
 548  $< z < 660 \text{ km}$ , region (2). Blue:  $1320 \text{ km} < x < 1980 \text{ km}$ ,  $660 \text{ km} < z < 1320 \text{ km}$ ,  
 549 region (3). Magenta:  $1980 \text{ km} < x < 2640 \text{ km}$ ,  $660 \text{ km} < z < 1320 \text{ km}$ , region (4).

550

551 **FIGURE 7** Simulation results for plate speeds of 20 cm/yr (models 5 and 6) at  
 552 a time of 14 Ma from the initiation of plate motion as for Figure 3

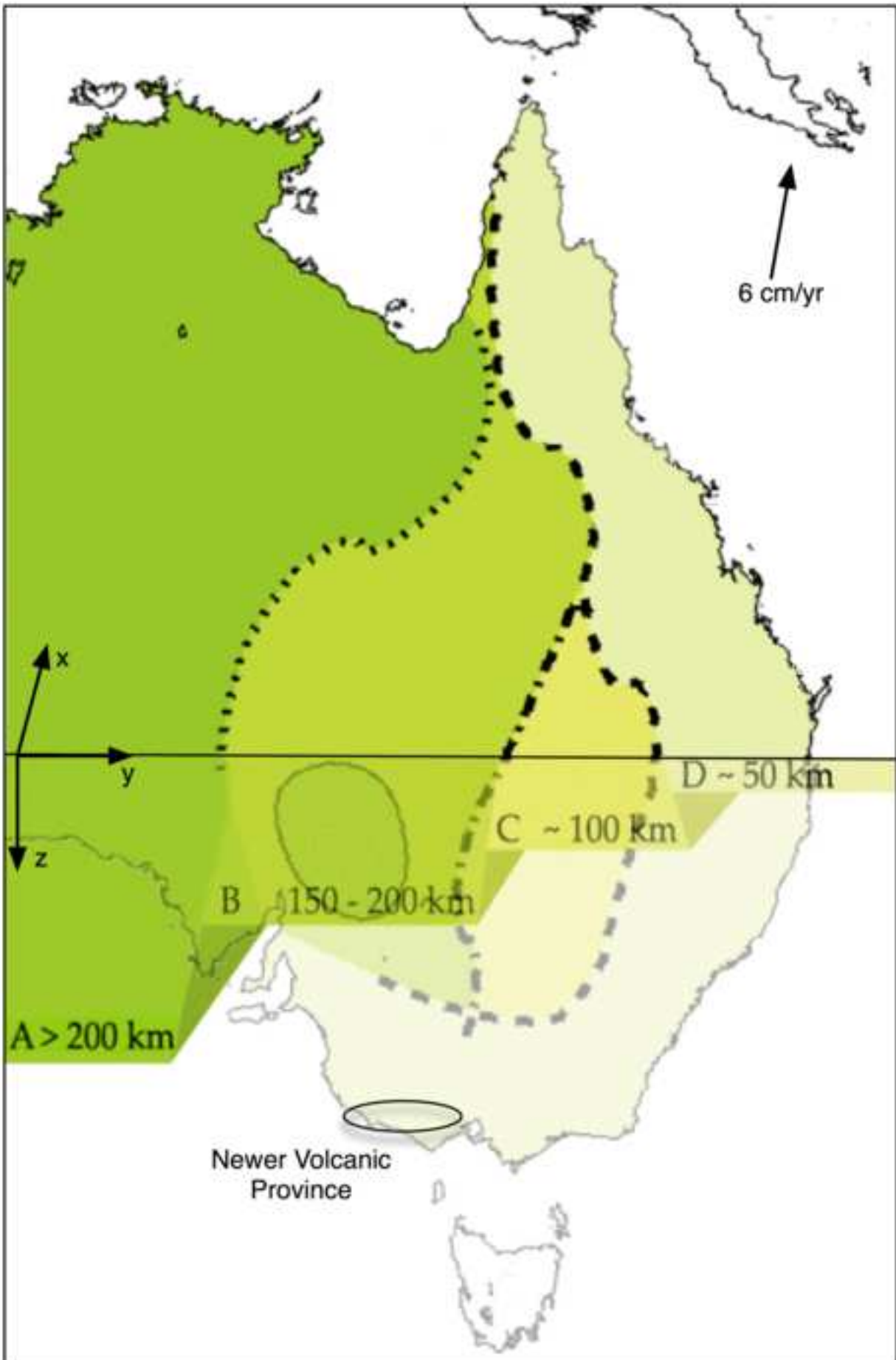
553

554 **TABLE 1** Model parameters including imposed plate speed, continental topog-  
 555 raphy and transient time. The time used for the 2.0 cm/yr and 20 cm/yr models is  
 556 the transient period, defined as the time taken for a parcel of mantle to travel along  
 557 the base of the upper mantle from the centre of the continent, ( $x = 0 \text{ km}$ ) past the  
 558 trailing edge to the periodic boundary ( $x = 2640 \text{ km}$ ). This time is 140 Ma for the  
 559 2.0 cm/yr model and 14.0 Ma for the 20 cm/yr model. It was found that the im-

560 posed plate speed of 0.2 cm/yr was not large enough to interact with the convective  
561 planform of the initial steady state model after 3.4 Ma as shown in Figure 3(a) and  
562 is therefore taken to be equivalent to the steady state model.

ACCEPTED MANUSCRIPT

Figure 1



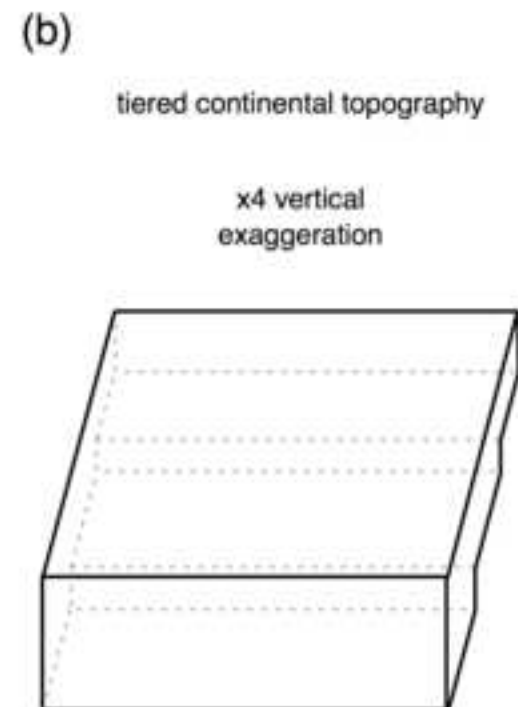
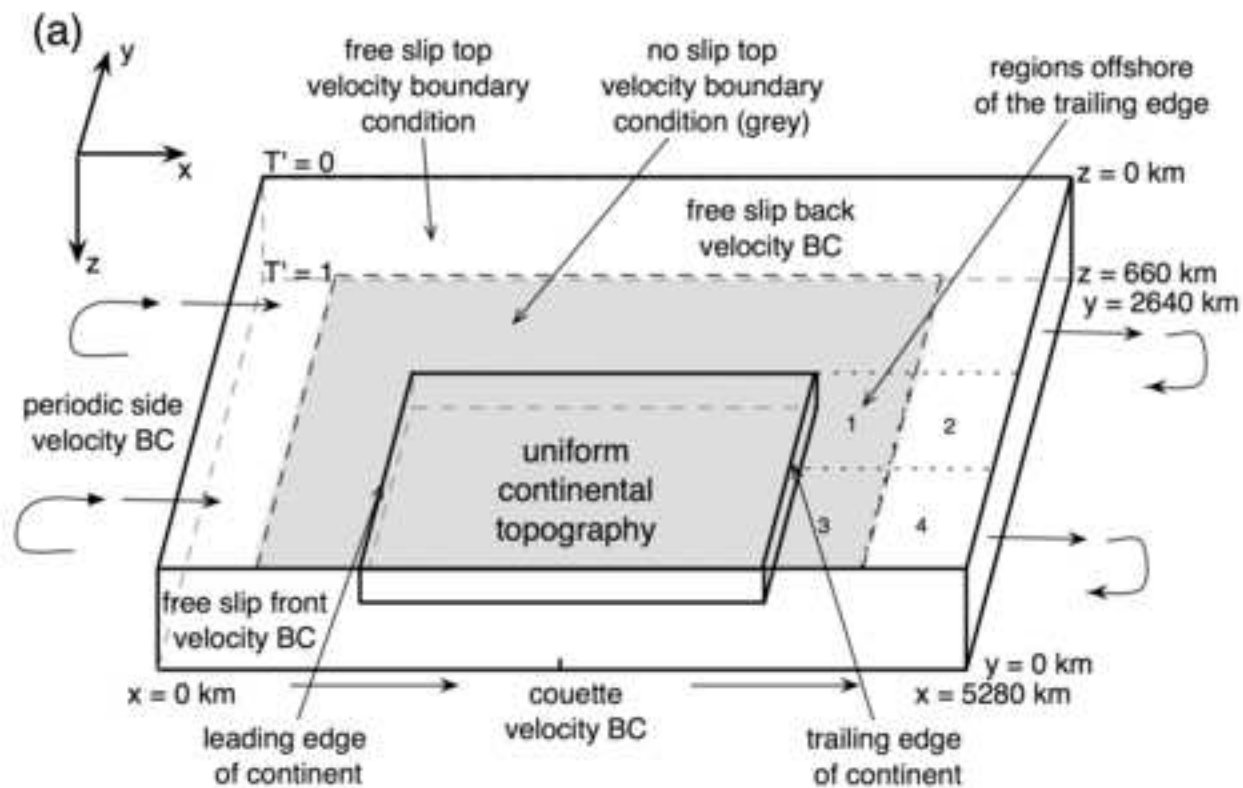


Figure 3

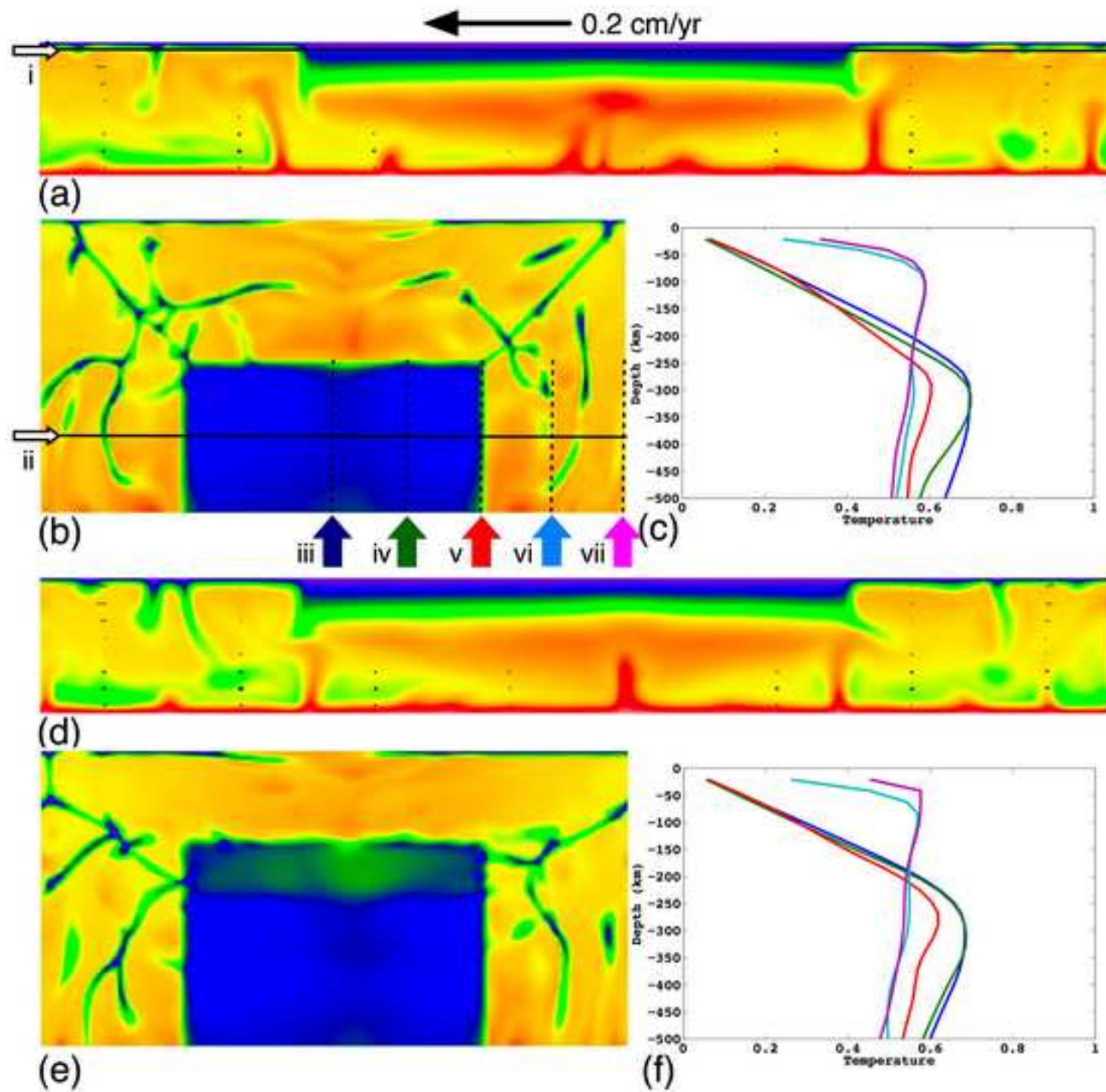
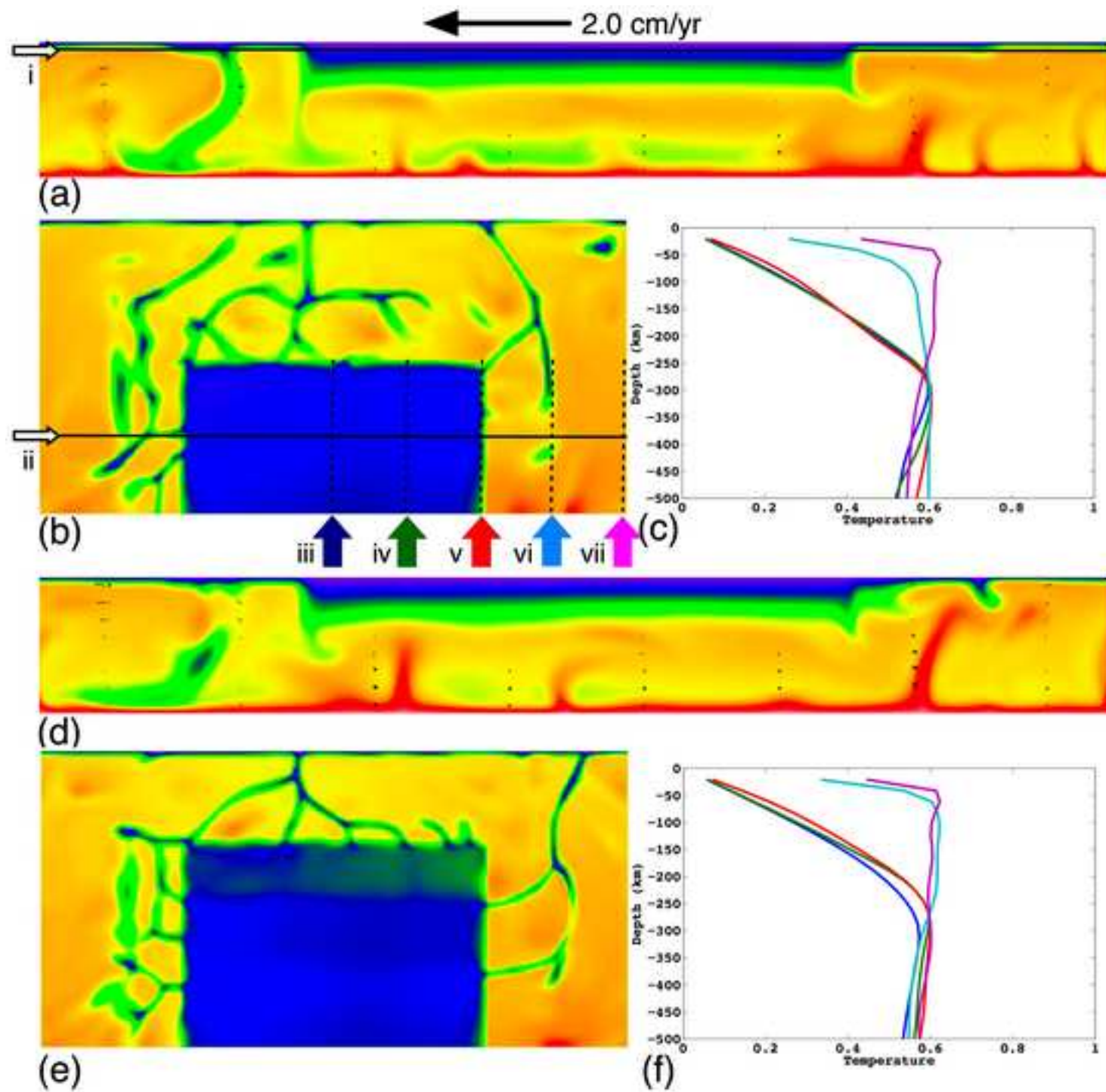


Figure 4



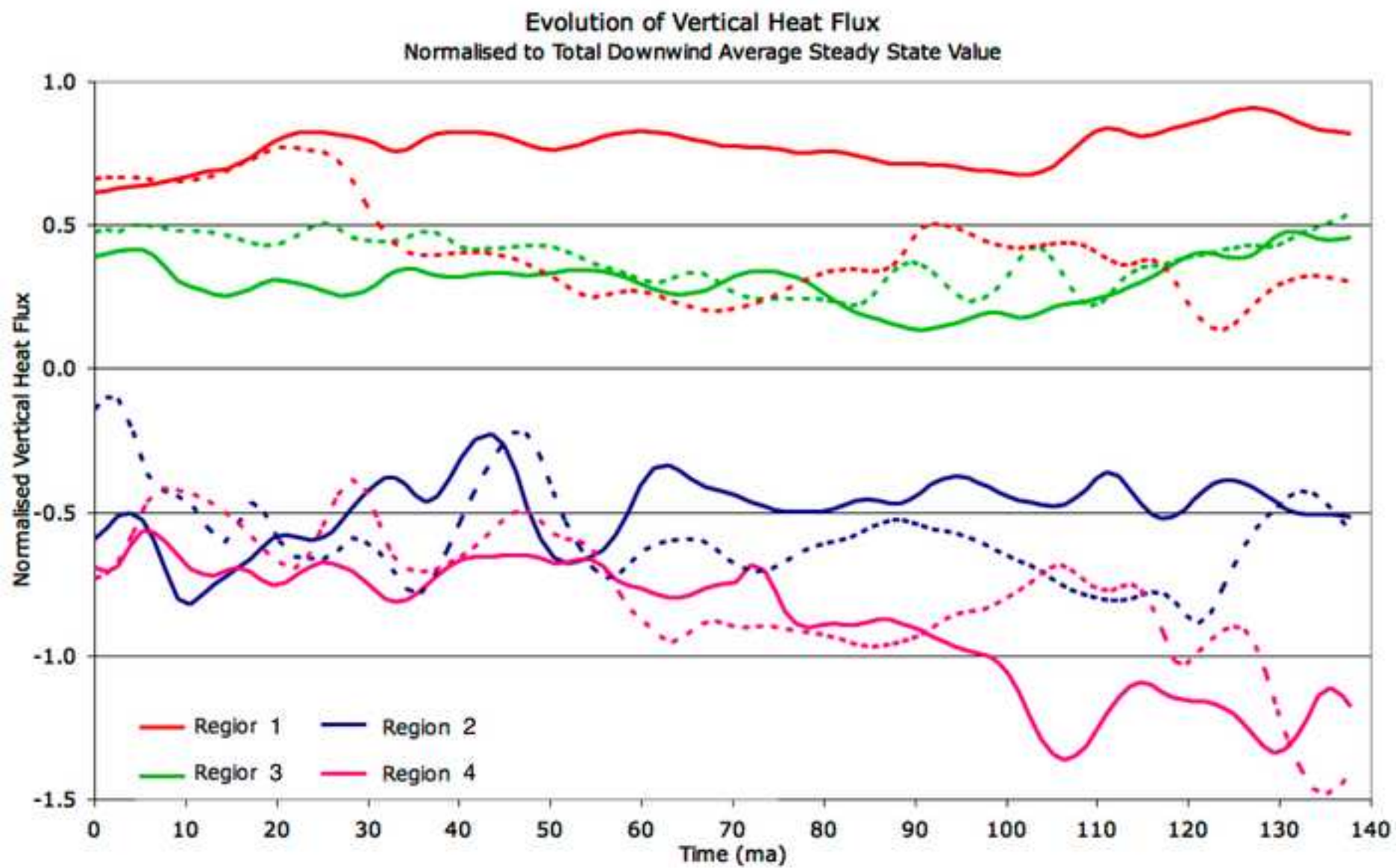


Figure 6

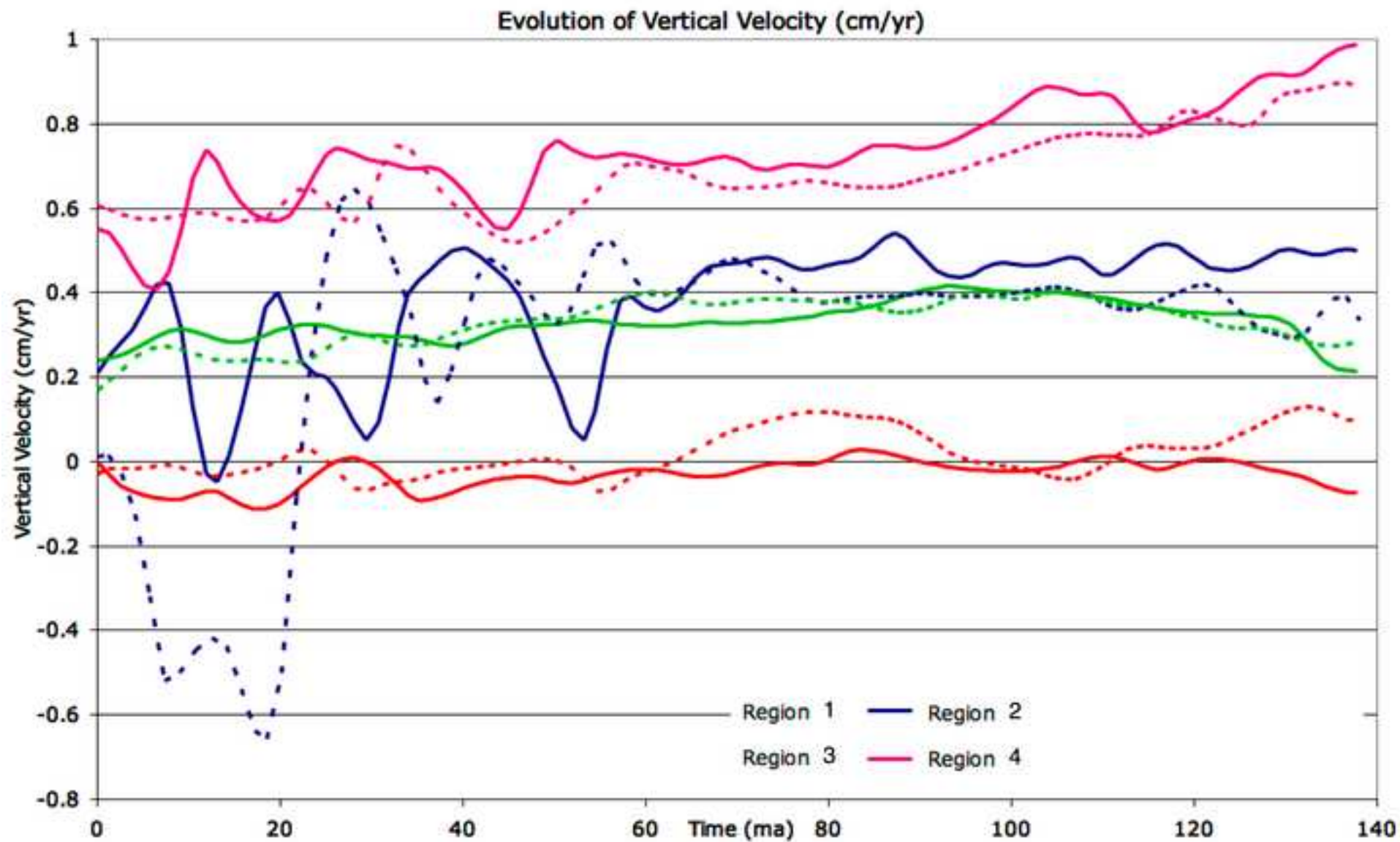
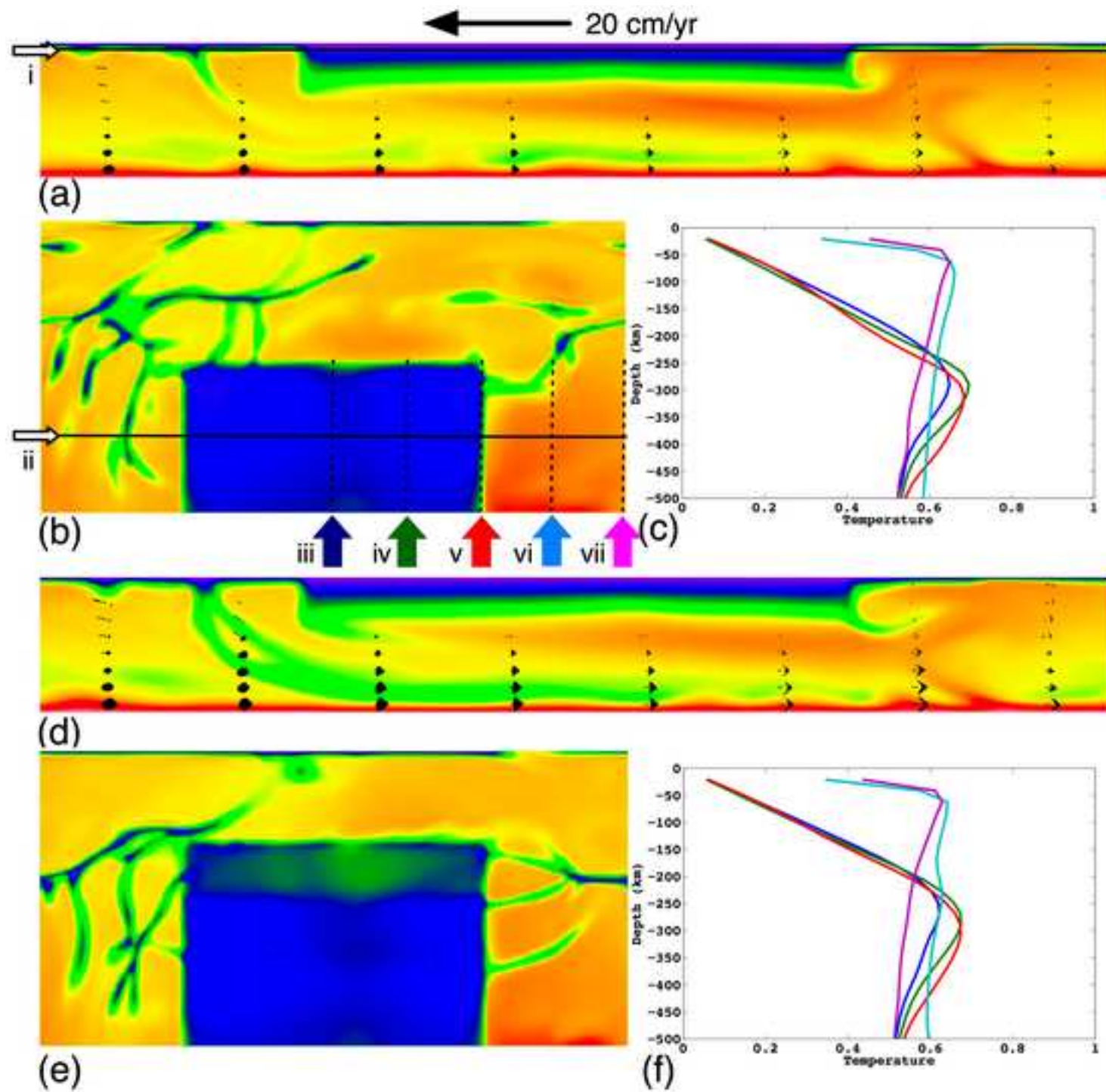


Figure 7



Model	Plate Speed	Topography	Transient Period
1	0.2 cm/yr	uniform	-
2	0.2 cm/yr	tiered	-
3	2.0 cm/yr	uniform	140 Ma
4	2.0 cm/yr	tiered	140 Ma
5	20 cm/yr	uniform	14 Ma
6	20 cm/yr	tiered	14 Ma